UAB
Universitat Autònoma
de Barcelona

Treball Final del Grau en Física

Metrology in the quantum regime: Fisher Information and Optimal Thermometry with Spin Networks

Alberto Rodriguez Rodriguez
Supervised by Dr. Martí Perarnau Llobet

- June 2025 -

Declaració d'autoria del Treball de Grau

Jo, Alberto Rodriguez Rodriguez, amb Document Nacional de Identitat 49223337W, i estudiant del Grau en Física de la Universitat Autònoma de Barcelona, en relació amb la memòria del treball de final de Grau presentada per a la seva defensa i avaluació durant la convocatòria de Juliol del curs 2024-2025, declara que:

- El document presentat és original i ha estat realitzat per la seva persona.
- El treball s'ha dut a terme principalment amb l'objectiu d'avaluar l'assignatura de treball de grau en física en la UAB, i no s'ha presentat prèviament per ser qualificat en l'avaluació de cap altra assignatura ni en aquesta ni en cap altra universitat.
- En el cas de continguts de treballs publicats per terceres persones, l'autoria està clarament atribuïda, citant les fonts degudament.
- En els casos en els que el meu treball s'ha realitzat en col·laboració amb altres investigadors i/o estudiants, es declara amb exactitud quines contribucions es deriven del treball de tercers i quines es deriven de la meva contribució.
- A l'excepció dels punts esmentats anteriorment, el treball presentat és de la meva autoria.

Signat:

Declaració d'extensió del Treball de Grau

Jo, Alberto Rodriguez Rodriguez, amb Document Nacional de Identitat 49223337W, i estudiant del Grau en Física de la Universitat Autònoma de Barcelona, en relació amb la memòria del treball de final de Grau presentada per a la seva defensa i avaluació durant la convocatòria de Juliol del curs 2024-2025, declara que:

- El nombre total de paraules (segons comptatge proposat) incloses en les seccions des de la introducció a les conclusions és de (9275) paraules.
- El nombre total de figures és de (6).

En total, el document comptabilitza:

(6135) paraules+(77)×20 paraules / línia de fórmula+(8)×200 paraules / figura = 9275 paraules,

que compleix amb la normativa al ser inferior a 10000[1].

Signat:

[1] S'ha fet servir l'eina de comptatge d'Overleaf, que considera cada equació en el text com 1 paraula. A més, només es comptabilitza el text entre la introducció i les conclusions, tal i com es detalla a la guia docent de l'assignatura.

Abstract

This thesis investigates the fundamental limits and practical aspects of temperature estimation in the quantum regime [1]. Starting from the framework of quantum estimation theory, we characterize the optimal equilibrium thermometer by maximizing the Quantum Fisher Information (QFI) over all possible energy spectra [2]. This yields a theoretical bound for thermometric precision. We then analyze physically motivated spin interaction models — the Star and All-to-All configurations — which were recently identified as optimal structures among generic spin networks [3]. By comparing their performance with the theoretical bound, we assess their suitability as realistic thermometric probes. Finally, we present new results in the context of dynamical quantum thermometry, studying how energy and QFI evolve during thermalization. Using numerical simulations of open quantum system dynamics, we find that while energy relaxes rapidly, QFI converges more slowly, revealing a trade-off between sensitivity and equilibration time. These results offer valuable insight into the design of efficient quantum thermometers and may inform applications in quantum sensing, thermodynamics, and precision measurements in out-of-equilibrium systems.

Acknowledgment

First of all, I would like to thank Dr. Martí Perarnau for all his guidance during the whole course. Even though it has been difficult, he always found some time for me, to help me with this interesting and challenging work.

Also, I want to mention the support of my colleagues, who have helped me through the 4 years that we have been studying this amazing degree, and with whom I have lived incredible experiences that I will never forget.

Last but not least, I would like to acknowledge my family, especially my mum and dad, for all the sacrifices they have made so that I could have all the opportunities they never had, I hope one day I can give you back everything you have given me.

Contents

Chapter 1

Introduction

1.1 Motivation

The precise control and manipulation of quantum systems has led to new developments in modern physics, particularly in scenarios involving extremely low temperatures. Achieving and measuring temperatures in the nanokelvin regime is now possible with ultra-cold atomic gases, but it presents both a technological and conceptual challenge, and new methods with atomic size probes are being developed. This emerging frontier has given rise to the field of ***quantum thermometry***, which seeks to determine the fundamental limits of temperature estimation in the quantum regime.

Although temperature is a familiar macroscopic concept, its formal definition becomes surprisingly difficult when applied to microscopic quantum systems. The existence of temperature, can be taken as the first steps in the axiomatic construction of thermodynamics, and all the well-established concepts like thermal equilibrium or efficiency of Carnot engines. However, when moving away from large Hamiltonian systems, these classical assumptions begin to fail. Quantum thermodynamics attempts to address this gap by redefining thermodynamic variables [4](such as heat, work, and temperature), or even reformulating the laws of thermodynamic, so that they remain meaningful at the quantum scale. In this context, quantum thermometry provides a theoretical framework for understanding how quantum systems can be used to infer temperature with optimal precision. One approach, that will be the one used in this work, involves weakly coupling a small quantum probe to a thermal system, allowing it to thermalise and then extracting temperature information from the probe alone. This is conceptually similar to how classical thermometers operate, but requires careful modeling of the quantum interactions involved. The framework also considers more general scenarios, including strong probe-system correlations and non-equilibrium dynamics, which can enhance sensitivity at ultra-low temperatures, but as a trade-off, one is required to develop a thorough comprehension of the dissipative interactions among them.

The precision of quantum thermometric protocols is typically bounded using tools from quantum estimation theory. These methods not only establish theoretical limits but also identify which observables or setups are most sensitive to temperature changes. Even when the optimal measurements are not experimentally accessible, sub-optimal but practical alternatives can be proposed.

Recent theoretical advances have shaped a unified view of quantum thermometry, enabling the comparison of diverse methods and the design of high-performance temperature probes. While experimental progress in nanoscale thermometry is rapidly advancing, this project will focus on some theoretical foundations and developments that brace the current understanding of temperature sensing in the quantum regime.

1.2 Structure

The thesis is organized as follows. In Chapter 2, we present the theoretical framework of quantum thermometry, introducing the concepts of Fisher Information, Quantum Fisher Information, and the general structure of equilibrium thermometers. Chapter 3 focuses on identifying the optimal quantum thermometer by maximizing the Quantum Fisher Information, and comparing this bound with the performance of realistic two-body spin network models. In Chapter 4, we extend the study to the dynamical regime, analyzing how thermometric quantities evolve during thermalization using open quantum system dynamics. Finally, in Chapter 5, we summarize the main conclusions and discuss possible applications and future directions.

Chapter 2

Theoretical framework

In this section, we introduce the essential concepts required to understand how metrology operates in the quantum regime, focusing on temperature estimation. We begin by outlining the fundamental challenges associated with defining and measuring temperature in quantum systems. Then, we present the key tools of quantum estimation theory that are employed to tackle these challenges.

2.1 Thermometry in the Quantum Regime.

Quantum thermometry is concerned with estimating temperature in regimes where quantum effects become significant. This problem arises naturally when dealing with systems of few particles or at ultra-low temperatures, where the traditional macroscopic notions of thermodynamics break down or become ambiguous.

The theoretical foundation of quantum thermometry rests on a statistical description of systems in *thermal equilibrium*. Such systems are modeled by the Gibbs density operator:

$$\varrho(T) = \frac{1}{Z}\sum_k e^{-\beta\varepsilon_k}|\varepsilon_k\rangle\langle\varepsilon_k|, \tag{2.1}$$

where $\beta = 1/k_B T$, $\{\varepsilon_k\}$ are the energy eigenvalues of the Hamiltonian H, and $Z = \sum_k e^{-\beta\varepsilon_k}$ is the partition function. For convenience, we hereafter set $\mathbf{k_B} = \hbar = \mathbf{1}$. The important fact to notice here is that temperature T is not an observable but a parameter to be estimated from measurements on the state $\varrho(T)$.

From this point of view, thermometry becomes a problem of parameter estimation, where quantum estimation theory provides a powerful framework. The central quantity of interest is the *Classical Fisher Information* (CFI). Given a system whose state $\varrho(\xi)$ depends on some unknown parameter ξ that we want to infer, the only way to obtain information is by performing measurements with a set of positive hermitian operators $\Pi = \{\Pi_m\}$. Then $p(\mathbf{x}|\xi)$ is the probability of obtaining the data set $\mathbf{x}$, being the value of the parameter exactly ξ. We can define the CFI of the set of measurements $\widehat{\mathbf{\Pi}}$ with respect to ξ as

$$\mathcal{F}_c(\widehat{\mathbf{\Pi}}, \xi) := \sum_{\mathbf{x}} \frac{(\partial_\xi p(\mathbf{x}|\xi))^2}{p(\mathbf{x}|\xi)}. \tag{2.2}$$

This quantity captures the response of the probability distribution $p(\mathbf{x}|\xi)$ to small changes in the parameter ξ. In other words, it tells us how sensitive the measurements are to changes in the parameter, so our objective is to find which measurements maximize this CFI, in order to determine the exact real value of ξ with maximum precision. Mathematically, the CFI bounds the precision of any unbiased estimator through the *Cramér-Rao bound* (CRB), given $\mathcal{N}$ independent measurements:

$$\Delta\xi_{est}(\widehat{\mathbf{\Pi}}) \geq \frac{1}{\sqrt{\mathcal{N}\mathcal{F}_c(\widehat{\mathbf{\Pi}}, \xi)}}, \tag{2.3}$$

Thus, our first objective will be to identify which set of measures maximize the CFI when the temperature is our parameter.

If we chose to perform projective measurements onto the eigenstates of some observable O to estimate ξ we can adapt the CRB to this case and obtain (for $\mathcal{N} = 1$) [5] [6] [7]

$$\frac{\Delta O}{|\partial_\xi \langle O \rangle|} \geq \frac{1}{\sqrt{\mathcal{F}_c(O, \xi)}}, \tag{2.4}$$

with $\langle O \rangle = \mathrm{tr}\{O\varrho(\xi)\}$.

However, in realistic situations, the optimal measurements may be impractical, in such cases, the *Quantum Fisher Information* (QFI) allows us to benchmark alternative protocols. QFI is simply the optimization of the CFI over all possible measurements $\mathcal{F}(\xi) = \max_{\widehat{\mathbf{\Pi}}} \mathcal{F}_c(\widehat{\mathbf{\Pi}}, \xi)$ or alternatively [8]

$$\mathcal{F}(\xi) := \mathrm{tr}\{\varrho(\xi)\, L_\xi^2\} \ , \tag{2.5}$$

where L_ξ is the symmetric logarithmic derivative (SLD), defined implicitly by

$$L_\xi \varrho(\xi) + \varrho(\xi) L_\xi := 2\partial_{\xi'} \varrho(\xi')\big|_{\xi'=\xi} \ . \tag{2.6}$$

and we can effectively use this equation to transform (2.4) into

$$\frac{\Delta O}{|\partial_\xi \langle O \rangle|} = \frac{\Delta O}{\mathrm{cov}(O, L_\xi)} \geq \frac{1}{\Delta L_\xi} = \frac{1}{\sqrt{\mathcal{F}(\xi)}} \tag{2.7}$$

where the covariance is defined by cov(A,B):= $\langle AB + BA \rangle/2 \ - \ \langle A \rangle \langle B \rangle$. The first equality follows directly from (2.6) using the satisfied condition that $\langle L_\xi \rangle = 0$, then we can apply the Cauchy-Schwartz inequality and (2.5) to obtain the last equality.

Now from (2.7) one can easily see that the ultimate precision bound is obtained when $O = L_\xi$. Thus we can establish that *the optimal estimator of ξ can be built from projective measurements onto the eigenbasis of the SLD of $\varrho(\xi)$*.

However, this type of measurements aren't always experimentally available. Then, sub-optimal measurements can be quantified by their CFI and compared to the QFI to assess their thermometric power.

2.1.1 Equilibrium thermometry

Now that we have introduced the basic quantum estimation tools needed, we can tackle the basic problem of estimating the temperature of a system in thermal equilibrium. As we just saw, the key element to build optimal thermometers is to find the SLD of our state $\varrho(T)$ in (2.1).

We consider an N-dimensional system with Hamiltonian

$$H = \sum_i^N \varepsilon_i \, |i\rangle \langle i| \tag{2.8}$$

in the equilibrium state (2.1) (this could also describe a thermalized probe in weak contact with the system). Then we can compute (detailed in (A.1))

$$\partial_T \varrho(T) = \frac{1}{T^2} \varrho(\langle H \rangle - H) \ , \tag{2.9}$$

and use it with (2.6) to obtain the SLD for the thermal state (detailed in (A.2)

$$\frac{1}{2}\{L_T, \varrho\} = \frac{1}{T^2} \varrho(\langle H \rangle - H) \to L_T = \frac{1}{T^2}(H - \langle H \rangle) \ . \tag{2.10}$$

So we can now establish that *energy measurements are optimal for temperature estimation* with a system(probe) in thermal equilibrium(thermalized).

With this result, we can introduce the calculated SLD in (2.5) to find that the QFI can be easily computed as

$$\mathcal{F}(T) = \mathrm{tr}[L_T^2\,\varrho(T)] = \mathrm{tr}\left[\left(\frac{1}{T^2}(H-\langle H\rangle\right)^2\varrho(T)\right] \tag{2.11}$$

$$= \frac{1}{T^4}\left(\mathrm{tr}[H^2\varrho(T)] - 2\langle H\rangle\,\mathrm{tr}[H\varrho(T)] + \langle H\rangle^2\,\mathrm{tr}[\varrho(T)]\right) \tag{2.12}$$

$$= \frac{1}{T^4}\left(\langle H^2\rangle - \langle H\rangle^2\right) = \frac{\Delta^2 H}{T^4}\ . \tag{2.13}$$

And the *quantum*-CRB becomes

$$\sqrt{\mathcal{N}}\Delta T \geq \frac{1}{\sqrt{\mathcal{F}(T)}} = \frac{T^2}{\Delta H} \tag{2.14}$$

which for $\mathcal{N}=1$ becomes the uncertainty relation

$$\Delta\beta\Delta H \geq 1\ . \tag{2.15}$$

Now, the QFI strongly depends on the energy structure, so one can ask which energy spectrum maximizes this energy variance, we will see that in section 3.1.

2.1.2 Thermometry out of equilibrium

We now need to tackle situations in which information about the temperature may be acquired only by local measurements on a small accessible fraction, called the *probe*. Despite this, one can still extract information about the global temperature T by measuring the probe.

Out of equilibrium, the Hamiltonian can be split as $H = H_p + H_S + H_I$, in probe, system and interaction terms respectively, and the reduced state of the probe, $\varrho_p = \mathrm{tr}_s\varrho$ does not necessarily follow a Gibbs distribution, specially if the interactions are strong. As a result, the uncertainty relation (2.15) does no longer hold. Nevertheless, it can be adapted to strong interactions by modifying the internal energy of the probe, and therefore the energy variance, this is explicitly derived in A.3.

Interestingly, this strong probe–system interactions, often avoided in weak-coupling thermometry, can be used as a thermometric resource. While such interactions complicate the dynamics and introduce correlations, they can reshape the probe's effective spectrum in a way that enhances thermal sensitivity. In fact, when the strength of the interaction increases, energy measurements become less informative about the temperature of the system, since the state of the probe is no longer a Gibbs state because of the interactions. This affects to the construction of the SLD, which is implicitly defined by the state of the probe by (2.6), and by extension also affects to the optimal measurements. See [9] for an example where another observable, more sensitive to temperature changes in the $T \ll 1$ regime, is found.

In this work, the interactions will be restricted to thermalising conditions, described in section 2.2.2, where the probe is weakly coupled to the system and strong interactions are not considered.

2.2 Dynamical Quantum Thermometry

In this section we focus on the out-of-equilibrium evolution of a quantum probe coupled to a thermal reservoir. In this approach, the probe is initially prepared in a given state ρ_0, and evolves under a temperature-dependent quantum channel $\mathcal{E}_T^t$, and measured at some finite time t.

For example, when the system evolves under *coherent unitary dynamics*, typically governed by temperature-dependent Hamiltonian, the system does not thermalise with the environment. Instead, it retains coherence throughout the process. This is useful for short interaction times as it avoids the loss of information through dissipation, and we can obtain a t^2-scaling of the

QFI [paper thermalization]. However, in the limit of large t the unitary evolution is hard to accomplish, and *steady-state metrology* offers an alternative framework.

Another used protocol is *interferometric thermometry*, where the probe (often a qubit) acquires a dynamical phase during the (weak) interaction with the environment. This gained phase encodes temperature information of the bath, and it has proven to be very sensitive for low-temperature thermometry [see [10][11][12][13] for exemples].

Finally we could also apply *external control fields* to the probe or dynamically switch the probe-bath coupling. These settings are used to enhance the sensitivity of the probe to the bath temperature, by choosing more precisely the temperature range of interest or accelerating convergence to optimal states.

In what follows we will explore in detail the framework of thermalising dynamics, where the probe is weakly coupled to a thermal bath and its evolution is described by the theory of Open Quantum Systems.

2.2.1 Open Quantum Systems

Before analyzing how thermometry is described under thermalising dynamics, we will introduce a few theoretical concepts about Open Quantum Systems, and the elements used in the next section. In general terms, an open system is a quantum system S which is coupled to another quantum system B called the environment or reservoir, so both are considered subsystems of the combined total system $B+S$, which is considered closed. The total system hamiltonian H describes how the total density matrix $\varrho(t)$ evolves in time, through the *von Neumann equation*

$$\frac{d}{dt}\varrho(t) = -i\,[H(t), \varrho(t)]\ . \tag{2.16}$$

However, we are interested in the system S evolution. If we approximate $\varrho(t) \approx \varrho_s(t) \otimes \varrho_B$, we have that $\varrho_s = \mathrm{tr}_B \varrho$, where tr_X means the partial trace on the subsystem X. Thus, *reducing* the equation to the system S we obtain

$$\frac{d}{dt}\varrho_s(t) = -i\,\mathrm{tr}_B\,[H(t), \varrho(t)]\ . \tag{2.17}$$

In general the dynamics of the reduced system defined by this two exact equations will be quite involved. Nevertheless, under the condition that the thermalization time is much longer than any other time scale, we formulate the reduced system dynamics in terms of a quantum dynamical semigroup. In this framework the evolution of ϱ_s is described by $V(t)$, the elements of the semigroup

$$\varrho_s(0) \longmapsto \varrho_s(t) = V(t)\varrho_s(0) \equiv \mathrm{tr}\{U(t,0)[\varrho_s(0)\otimes\varrho_B]U^\dagger(t,0)\}\ , \tag{2.18}$$

where $U(t,t_0) = \exp[-iH(t-t_0)]$.

Under certain mathematical conditions [14] a linear map $\mathcal{L}$, the generator of the semigroup, allows us to represent the elements in the exponential form $V(t) = \exp[\mathcal{L}t]$, what yields to the *Markovian quantum master equation* or *Lindblad equation*

$$\frac{d}{dt}\varrho_s(t) = \mathcal{L}\varrho_s(t)\,. \tag{2.19}$$

In the most general form, the generator, often called *Lindbladian*, is defined as

$$\mathcal{L}\varrho_s = -i[H,\varrho_s] + \sum_{k=1}^{N^2-1}\gamma_k\left(A_k\varrho_s A_k^\dagger - \frac{1}{2}A_k^\dagger A_k\varrho_s - \frac{1}{2}\varrho_s A_k^\dagger A_k\right) \tag{2.20}$$

where the set of operators $\{A_k\}$, known as Lindblad operators, can be founded by the decomposition of H_I^S, that is the system part of of H_I^S, i.e $H_I = H_I^S \otimes H_I^B$, and they encode the dissipative effects of the interaction system-bath. γ_k play the role of relaxation rates for the different decay modes of the open system.

2.2.2 Thermometry under thermalising dynamics

Considering now that the environment is a heat bath at inverse temperature β, in the absence of external time-dependent fields, we expect the Gibbs state

$$\varrho_{th} = \frac{e^{-\beta H_s}}{\mathrm{tr}_S[e^{-\beta H_s}]} \tag{2.21}$$

to be a stationary solution of the equation (2.19). It can be shown then that for any initial state the system returns to equilibrium

$$\varrho_s(t) \to \varrho_{th} \ , \ \text{for } t \to +\infty \tag{2.22}$$

since the quantum dynamical semigroup has the property of being ergodic.

If the spectrum of the system Hamiltonian $H_s = \sum_n \varepsilon_n |n\rangle \langle n|$ is non-degenerate it gives a closed equation of motion for the populations

$$P(n,t) = \langle n| \varrho_s(t) |n\rangle \tag{2.23}$$

of the $|n\rangle$ eigenstate. Thus, the equation for the diagonals of the density matrix in the eigenbasis of H_s and the populations are governed by the equation

$$\frac{d}{dt}P(n,t) = \sum_m \left[W_{m\to n}P(m,t) - W_{n\to m}P(n,t)\right]. \tag{2.24}$$

This equation is of the form of the classical discrete master equation with time-independent transition rates given by

$$W_{m\to n} = \sum_{\alpha,\beta} \gamma_{\alpha\beta}(\varepsilon_m - \varepsilon_n)\langle m|A_\alpha|n\rangle\langle n|A_\beta|m\rangle. \tag{2.25}$$

For thermal equilibrium systems (with NO degeneracy) in the thermodynamic limit this rates (2.25) fulfill the condition [14]

$$W_{n\to m}\exp(-\beta\varepsilon_n) = W_{m\to n}\exp(-\beta\varepsilon_m) \ , \tag{2.26}$$

which is known as the condition of *detailed balance*, and which leads to the conclusion that the equilibrium populations follow the Boltzmann distribution

$$P(n, t = t_{eq}) = \text{const} \times \exp(-\beta\varepsilon_n) \tag{2.27}$$

over the energy eigenvalues ε_n. In other words, that the state in equilibrium is described by the Gibbs state (2.21).

Chapter 3

Optimal Quantum Thermometry

Now that we have established the theoretical foundations to understand how thermometry works in the quantum regime, we turn our attention into what makes a thermometer truly optimal. We will explore the conditions that maximize the information we can extract about temperature, and once we have laid out those theoretical limits, we will shift our focus to more accessible, realistic systems—with spin networks—that can get us as close as possible to that optimal performance.

3.1 Optimal spectrum for equilibrium thermometry

In previous sections we obtained the relation for the QFI of a Gibbs state like (2.1)

$$\mathcal{F}(T) = \frac{\Delta^2 H}{T^4} \tag{3.1}$$

so our objective now is to find which energy spectrum $\{\varepsilon_i\}$ maximizes the energy variance, in order to find de maximum QFI and by extension the optimal system for temperature estimation.

3.1.1 Fisher Information

Before starting the search for the optimal spectrum, it is important to mention that since we are working with the optimal measurements (energy measurements) on a diagonal state like (2.1), we can indistinguishably talk about classical and quantum Fisher Information, since they are the same in this specific case. In A.4 the CFI is derived and proved to be equal to the QFI founded in section 2.1.1.

To find this spectrum we need to impose that $\partial_{\epsilon_i}\Delta^2 H = 0$ in order to find what set of $\{\varepsilon_i\}$ maximizes it. For a general N-level probe the energy variance writes as

$$\Delta^2 H = \langle H^2\rangle - \langle H\rangle^2 = \sum_i^N \varepsilon_i^2 \frac{e^{-\beta\varepsilon_i}}{\mathcal{Z}} - \left(\sum_i^N \varepsilon_i \frac{e^{-\beta\varepsilon_i}}{\mathcal{Z}}\right) \tag{3.2}$$

By imposing $\partial_{\epsilon_i}\Delta^2 H = 0$ we obtain a set of N transcendental equations [15]. Subtracting the j-th equation from the i-th one we obtain the condition

$$(\epsilon_i - \epsilon_j)\left(\epsilon_i + \epsilon_j - 2 - 2\frac{\langle H\rangle}{T}\right) = 0. \tag{3.3}$$

That is, any two energy eigenvalues must be either equal or sum up to the same value at the stationary point of $\Delta^2 H$. This can only happen in a two-level system with energies ϵ_+ and ϵ_-, with N_0 degeneracy on the ground state and $N - N_0$ on the excited one. Since we can shift our energy spectrum in a way that $\epsilon_- = 0$, the dimensionless optimal gap is defined as

$$x^*_{N,N_0} \equiv \frac{\Omega^*}{T} = \frac{(\epsilon_+ + \epsilon_-)}{T} = 2\left(1 + \frac{\langle H\rangle}{T}\right). \tag{3.4}$$

We can rewrite this optimal gap with another expression (derived in A.5):

$$e^{x^*} = \frac{N - N_0}{N_0} \frac{x^* + 2}{x^* - 2}. \tag{3.5}$$

We will use this equation to numerically find the optimal gap for the different values of N. Then, using (3.4), we can calculate the difference [2]

$$\Delta^2 H_{N,N_0-1} - \Delta^2 H_{N,N_0} = \frac{1}{4}(x^{*2}_{N,N_0-1} - x^{*2}_{N,N_0}) \ , \tag{3.6}$$

that is always positive, since $x^{*2} \propto \langle H \rangle^2$ and $\langle H \rangle_{N,N_0-1} > \langle H \rangle_{N,N_0}$. Then we can conclude that if we want to maximize the energy variance, the degeneracy of the excited state must be the largest possible. In other words, the optimal probe that maximizes $\Delta^2 H$ and the FI is with $\mathbf{N_0 = 1}$. Thus, the Hamiltonian has the form:

$$H_{opt} = 0 \left|0\right\rangle \left\langle 0\right| + \sum_i^{D-1} \Omega \left|i\right\rangle \left\langle i\right| \tag{3.7}$$

where D is dimension of the Hilbert space.

Now, knowing the hamiltonian, we can easily compute the partition function:

$$\mathcal{Z} = 1 + (D-1)e^{-x}, \tag{3.8}$$

Then we can obtain the energy variance of the optimal spectrum

$$\Delta^2 H = \mathcal{Z}^{-1} \sum_i^D \epsilon_i^2 e^{-\epsilon_i/T} - (\mathcal{Z}^{-1} \sum_i^D \epsilon_i^{-\epsilon_i/T})^2 \tag{3.9}$$

$$= \frac{(D-1)\Omega^2 e^{-x}}{1 + (D-1)e^{-x}} - \frac{(D-1)^2 \Omega^2 e^{-2x}}{(1 + (D-1)e^{-x})^2} \tag{3.10}$$

$$= e^x \Omega^2 \frac{D-1}{(D - 1 + e^x)^2} \ . \tag{3.11}$$

And finally, the expression for the FI for different values of D

$$\mathcal{F}_D(T) = \frac{\Delta^2 H}{T^4} = \frac{e^x x^4}{\Omega^2} \frac{D-1}{(D-1+e^x)^2} \ , \tag{3.12}$$

which is maximal at $x = x^*_{N,1}$.

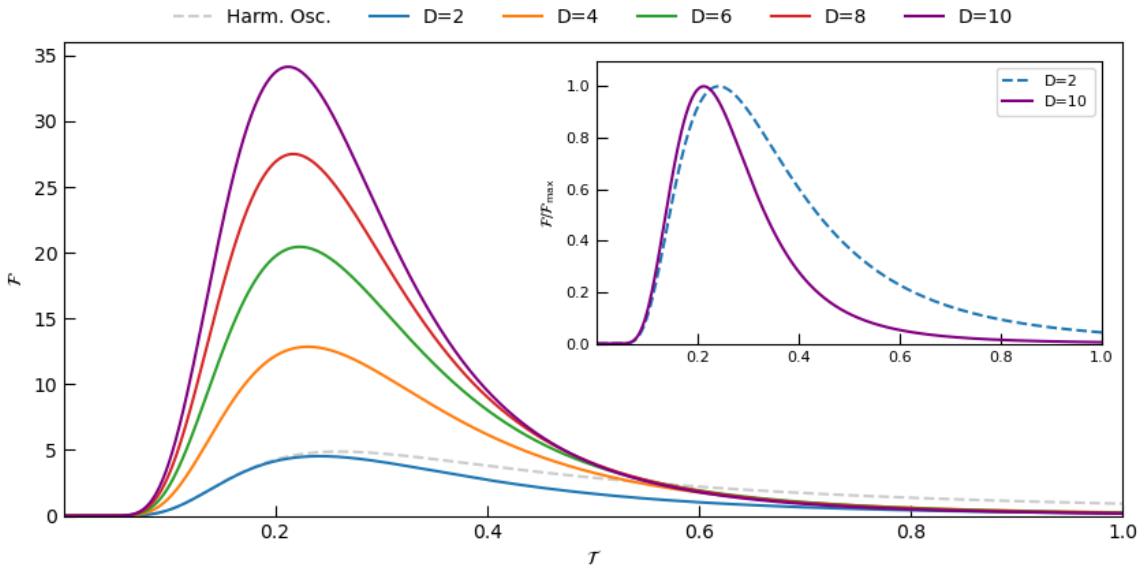

Figure 3.1: Fisher Information as a function of T for different values of N. Both T and $\mathcal{F}$ expressed in arbitrary units and fixing $\Omega = 1$.

In Figure (3.1) we can see the FI (3.12) for different values of D. As expected, the FI grows with D, and its maximum is practically at the same point for all the represented values. However, we also have a normalized version of the FI, comparing $D = 2$ and $D = 10$ to notice that, although $D = 10$ gives a higher FI, the specified temperature range where the probe is *efficient* is wider for $D = 2$.

3.1.2 Heat Capacity

Classical thermodynamics tells us that *heat capacity* is closely linked to temperature variations. In this section, we explore how this quantity can provide useful insight in the context of quantum thermometry. A general definition of the heat capacity is given by:

$$\mathcal{C}(T) = \frac{\partial U}{\partial T} = \frac{\partial \langle H \rangle}{\partial T}, \tag{3.13}$$

where $U = \langle H \rangle$ is the internal energy of the system. For a general 2-level system, with N_0 particles in the ground state ($\epsilon_1 = 0$) and $N - N_0$ on the excited one ($\epsilon_2 = \Omega$), the partition function becomes $\mathcal{Z} = N_0 + (N - N_0)e^{-\frac{\Omega}{T}}$, thus

$$\langle H \rangle = T^2 \partial_T \ln \mathcal{Z} = T^2 \frac{\partial_T \mathcal{Z}}{\mathcal{Z}} = \frac{(N - N_0)\Omega e^{-\frac{\Omega}{T}}}{N_0 + (N - N_0)e^{-\frac{\Omega}{T}}} \tag{3.14}$$

and the heat capacity for the optimal probe (i.e $N_0 = 1$ and, for now, N = D):

$$\mathcal{C}^{opt}(T) = \frac{\partial \langle H \rangle}{\partial T} = \frac{\partial}{\partial T}\left[\frac{(D-1)\Omega e^{-\frac{\Omega}{T}}}{1 + (D-1)e^{-\frac{\Omega}{T}}}\right] \tag{3.15}$$

$$= (D-1)\Omega \left[\frac{\left(\frac{\Omega}{T^2}\right) e^{-\frac{\Omega}{T}} \left(1 + (D-1)e^{-\frac{\Omega}{T}}\right) - e^{-\frac{\Omega}{T}}(D-1)e^{-\frac{\Omega}{T}} \left(\frac{\Omega}{T^2}\right)}{\left(1 + (D-1)e^{-\frac{\Omega}{T}}\right)^2}\right] \tag{3.16}$$

$$= \frac{\Omega^2}{T^2} \frac{(D-1)e^{-\frac{\Omega}{T}}}{\left(1 + (D-1)e^{-\frac{\Omega}{T}}\right)^2} = e^x x^2 \frac{D-1}{(D-1+e^x)^2} \tag{3.17}$$

$$= \frac{\Delta^2 H}{T^2} \ . \tag{3.18}$$

In the last step we have used (3.11). With this result and (3.12), we establish an important relation between the heat capacity and the FI:

$$\mathcal{F}(T) = \frac{\mathcal{C}(T)}{T^2} \ . \tag{3.19}$$

We can also find another useful expression for the heat capacity of the optimal probe. In the asymptotic limit of $D \to \infty$ the optimal gap becomes

$$e^{x^*} = (D-1)\frac{x^* + 2}{x^* - 2} \to x^* = \ln(D-1) + \ln\left(\frac{x^* + 2}{x^* - 2}\right) \approx \ln(D) \, . \tag{3.20}$$

Introducing this result into the heat capacity we can see how $\mathcal{C}^{opt}$ behaves in the limit of large probes.

$$\mathcal{C}^{opt}(D) = e^x x^2 \frac{D-1}{(D-1+e^x)^2} \sim \frac{(\ln D)^2}{4} \tag{3.21}$$

This optimal scaling of heat capacity represents our theoretical limit, which also applies to the FI. In the next section, we will explore real systems with two-body local interactions, aiming to find those that approach this bound as closely as possible.

3.2 Sub-Optimal spin-network thermometers

To initiate this search, we consider a generic system of spins with two-body interactions, described by a Hamiltonian of the form:

$$H = \sum_{i}^{N} h_i \sigma_i^z + \sum_{i<j}^{N} J_{ij} \sigma_i^z \sigma_j^z \tag{3.22}$$

where $\sigma_i^z = \pm 1$ is the i-th classical spin of the system. What we have to tackle now is the complexity of maximizing $\mathcal{C}$ (or identically $\Delta^2 H$) over all control parameters h_i and J_{ij}, to check if it is possible to achieve the optimal scaling $\mathcal{C} \propto N^2$ with physically motivated 2-body interactions. That scaling appears when we describe a spin system with (3.21), we have $D = 2^N$, where N is the total number of spins. Then the ultimate limit reads (in the asymptotic limit of $N \to \infty$):

$$\mathcal{C}^{opt}(2^N) \sim \frac{N^2 (\ln 2)^2}{4} \ . \tag{3.23}$$

Since we have already seen in 3.18, the heat capacity $\mathcal{C}$ only depends on the energy spectrum, so we must find the values of h_i and J_{ij} that maximize $\Delta^2 H$. This is a challenging task, that has already been addressed in [3], we will use the results that they have obtained via Machine Learning techniques. After repeating the optimization for different numbers of spins N, there were two patterns detected. For $N \in [2, 6]$, the *All-to-All* model performed slightly better than the other system found, the *Star Model*, which becomes the preferred choice for $N \geq 7$. These two systems are described by

$$H_{Star}(a, b) = a\sigma_1^z + b \sum_{i=2}^{N} \sigma_i^z (\mathbf{I} + \sigma_1^z) \tag{3.24}$$

$$H_{all}(h, J) = -h \sum_{i}^{N} \sigma_i^z - J \sum_{i<j}^{N} \sigma_i^z \sigma_j^z \tag{3.25}$$

where $a, b \in \mathbb{R}$, different for each value of N [3], describes how a single spin σ_1^z is uniformly coupled to the other ones, and same for h and J.

3.2.1 Star Model

We will focus first on the Star Model. With this Hamiltonian, we can distinguish two main classes of eigenstates, depending on the value of σ_1^z. If the first is spin up ($\sigma_1^z = +1$) and k spins also up, among the remaining $N-1$ ones, we have a $\binom{N-1}{k}$-degenerate evenly spaced states with energy

$$E_k = a + 2b(k - (N - 1 - k)) \ ; \ \ k = 0, ..., N - 1 \, . \tag{3.26}$$

On the other hand, if we have the first spin down ($\sigma_1^z = -1$) the second term of (3.24) vanishes independently of the value of all other spins $i \geq 2$, what gives us a 2^{N-1}-degenerate excited state with fixed energy

$$E_{\text{deg}} = -a \ \ . \tag{3.27}$$

Therefore, we can understand that the first spin acts as a switch, that turns on and off the effective magnetic field on the remaining spins.

Now, we can analytically compute the partition function of the Star Model by summing the two partition functions of $\sigma_1^z = \pm 1$ (explicitly derived in A.6)

$$Z_{\text{star}} = 2^{N-1} (e^{-\beta a} \cosh(2\beta b)^{N-1} + e^{\beta a}) \tag{3.28}$$

With this result we can easily compute the energy variance, and using (3.18) find the heat capacity for the Star Model and compare it with the optimal probe. Since

$$\Delta^2 H = \frac{\partial^2}{\partial \beta^2} \ln Z \tag{3.29}$$

we must now differentiate twice the partition function to find the energy variance of this configuration. Thus, introducing (3.28) and setting $\beta = 1$:

$$\Delta^2 H_{Star} = \frac{\partial^2}{\partial \beta^2} \ln \left[2^{N-1} (e^{-\beta a} \cosh(2\beta b)^{N-1} + e^{\beta a}) \right] \Big|_{\beta=1} \tag{3.30}$$

$$= \frac{4b^2(N-1)\cosh(2b)^N + 2e^{2a}\cosh(2b)\left(a^2 - b^2(N-1)(N-3)\right)}{\cosh(2b)^{2-N}\left(e^{2a}\cosh(2b) + \cosh(2b)^N\right)^2} +$$

$$+ \frac{(a^2 + b^2(N-1)^2)\cosh(4b) - 2ab(N-1)\sinh(4b)}{\cosh(2b)^{2-N}\left(e^{2a}\cosh(2b) + \cosh(2b)^N\right)^2} \tag{3.31}$$

So we can compute (since β is fixed to 1) the heat capacity by $\mathcal{C}_{Star}(N) = \Delta^2 H_{Star}$, and compare it with the optimal bound (Fig.3.2). It is also useful to compare the asymptotic limit of this two systems. For $N \to \infty$ we can approximate (3.31) to [3]

$$\mathcal{C}^{Star}_{max}(2^N) \sim \frac{(N-1)^2(\ln 2)^2}{4} = C^{opt}(2^{N-1}) \tag{3.32}$$

Which for large N becomes indistinguishable to the theoretical bound of (3.23), as we can see in Fig.3.2. We can establish the following relation to compare this systems:

$$\mathcal{C}^{opt}(2^{N-1}) \leq \mathcal{C}^{star}_{max}(2^N) \leq \mathcal{C}^{opt}(2^N) \tag{3.33}$$

3.2.2 All-To-All Model

Now, focusing on the All-to-All Hamiltonian of (3.25), we can notice that it is completely symmetric under permutations of the spin operators. This allows us to express the energy spectrum as a function of the total number n of spins up. Similar as we had in the Star Model, each level has a $\binom{N}{n}$-degeneracy with energy

$$E_n = h(N - 2n) + \frac{J}{2}[4n(N-n) - N(N-1)] \tag{3.34}$$

What gives us a partition function

$$Z_{all} = \sum_i g_i e^{-\beta E_I} = \sum_{n=0}^{N} \binom{N}{n} e^{-\beta E_n} \tag{3.35}$$

As it has been found in [3] the optimal values for h and J, that maximize $\mathcal{C}$ must satisfy the relation $h = J$. Introducing this constraint in (3.34) gives us

$$E_n = J\left[-\frac{N(N+1)}{2} + 2(n+1)(N-n) \right] = J\left[E_{n=N} + 2(n+1)(N-n) \right] \tag{3.36}$$

where the last equality means that the ground state is for $n = N$ and the excited states going parabolic in n.

In order to compare this system with the previous two, we cannot derive a direct analytical expression for the maximum heat capacity $\mathcal{C}^{\text{all}}_{\text{max}}$ as a function of N, as we did for the Star Model. This is because the partition function $\mathcal{Z}_{\text{all}}$ does not have a simple closed-form expression in terms of N. Instead, for each $N \in [2, 10]$, we numerically compute the energy spectrum using (3.36), then evaluate the partition function via (3.35), and finally obtain the energy variance through (3.29). Fixing $\beta = 1$, this variance corresponds directly to the heat capacity. All these steps are carried out with J treated as a variable parameter; we then determine $\mathcal{C}^{\text{all}}_{\text{max}}(n_i)$ by selecting the maximum of $\mathcal{C}(J)$. The data obtained is provided in B.1.

The following figures summarize, in a visual way, the computations and results discussed above. In the main plot, we observe that the Star Model becomes nearly indistinguishable from the theoretical bound as N increases, as expected. In contrast, for small probes, the All-to-All model offers slightly better performance.

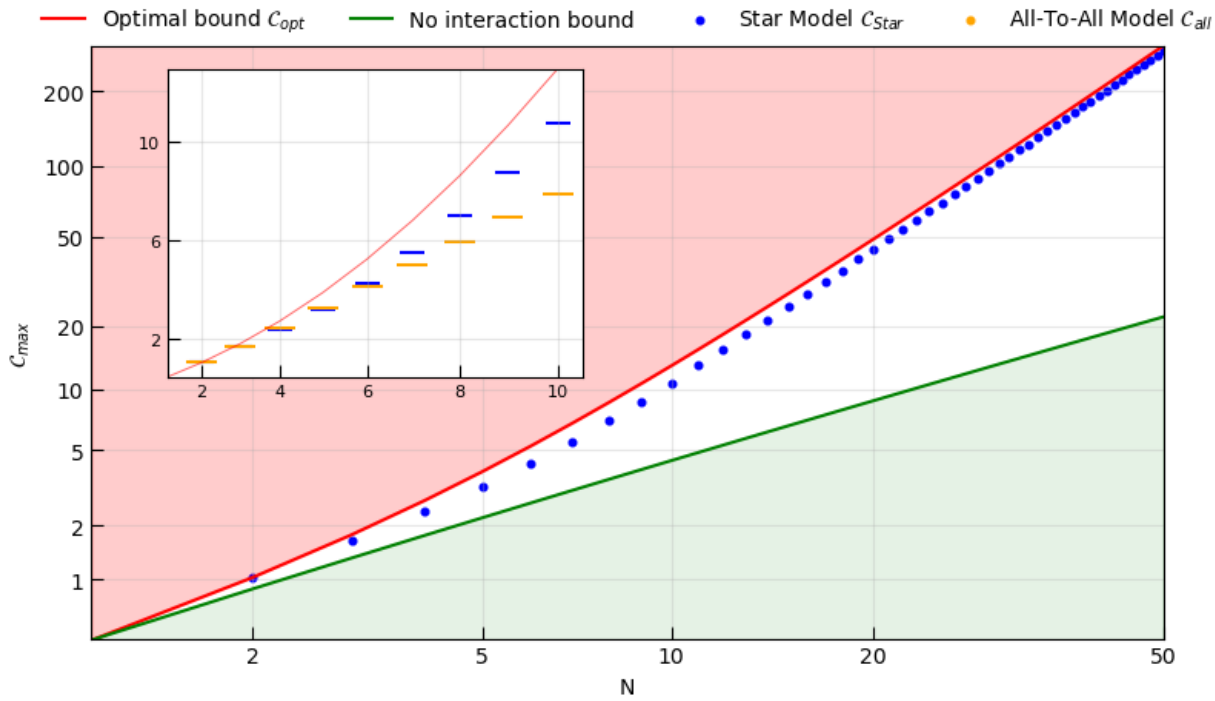

Figure 3.2: Maximum heat capacity of different spin-based systems. The red line corresponds to the optimal probe, described by (3.17), using the gap x numerically calculated by (3.5). The blue dots represent the Star Model described by (3.31), introducing the values for a and b from [3]. And just for a visual help we included the non-interactive lower bound in a green line, that represents $\mathcal{C}_{non-int} \approx 0.44N$, given that 0.44 is the maximum heat capacity for a single spin. In the smaller plot we can see in orange lines the heat capacity for the All-to-All model, using the data from B.1, which is bigger than the Star Model for $N \leq 5$.

Chapter 4

Transient regime: thermalization and steady state

Up to this point, we have been following known results, to identify the configuration of the theoretically optimal quantum probe and then optimized two-body spin interactions to obtain sub-optimal—but more experimentally feasible—thermometers. However this analysis has been restricted to the framework of thermal equilibrium, where the probe is assumed to be in a Gibbs state. In practice, optimizing the Fisher Information may come with the cost of longer thermalization time. This is what motivates the present section, where we develop **new results** by shifting our focus to the dynamical and steady-state behavior of these systems, when they are coupled to a thermal bath. Our goal is to investigate how both the energy and the Fisher Information, our primary figure of merit, evolve over time, and to analyze the trade-offs that appear when we try to optimize thermometric performance at equilibrium.

4.1 Relaxation to equilibrium

To study this evolution, we restrict ourselves to the conditions described in Sections 2.2.1 and 2.2.2. The systems are assumed to be weakly coupled to a thermal bath, and are therefore described by the Lindblad quantum master equation (2.19), while the population dynamics are governed by the Pauli master equation (2.24).

For simplicity, all derivations will be carried out assuming an initial product state with uniform populations, $p_n = 1/(N+1)$. As mentioned in Section 2.2.2, altering this initial condition does not affect the long-time behavior of the system, since the quantum dynamical semigroup is ergodic. This implies that, for a given generator $\mathcal{L}$, there exists a unique stationary state. For our generator, the Lindblad super-operator, that is constructed to satisfy detailed balance, this unique fixed point is the Gibbs state [14].

To study how the energy and the Fisher Information evolve during thermalization, we must first understand how the state populations change over time. Our initial objective is therefore to derive the rate equations that govern this evolution.

We assume that each qubit is individually coupled to the thermal bath, similar to the well-known model of Glauber spin dynamics in statistical physics. This implies that only transitions between adjoint levels can happen, i.e $W_{n\to n+l} = 0$ for $l \neq \pm 1$. This type of interaction leads the transition rates in (2.25) to take the form (see e.g. [16]):

$$W_{n\to m} = \alpha\xi_n \left(1 + e^{\beta\Delta U}\right)^{-1} \quad , \tag{4.1}$$

where α is the thermalization rate, ξ_n is a factor that depends on the degeneracy of level n, and ΔU is the energy difference associated with the transition. And the equations for the probabilities in (2.24) become

$$\dot{p}_n = -p_n[W_{n\to n+1} + W_{n\to n-1}] + p_{n+1}W_{n+1\to n} + p_{n-1}W_{n-1\to n} \tag{4.2}$$

Focusing first on the Star Model, we have two types of eigenstates. Denoting by n the number of spins up, if $n = 0$, it means that the central spin is also down, and the state corresponds to an energy $E_0 = -a$ with degeneracy $g_0 = 2^{N-1}$. For $n \geq 1$, using $k = n - 1$, the energies E_k are given by (3.26), with degeneracies $g_k = \binom{N-1}{k}$. Using this, transition rates can be written as

$$W^{Star}_{0\to 1} = \alpha \left(1 + e^{\beta \Delta U}\right)^{-1} \; ; \; W^{Star}_{n\to n+1} = \alpha(N-n) \left(1 + e^{\beta \Delta U}\right)^{-1} \quad \text{for } n \geq 1 \tag{4.3}$$

$$W^{Star}_{1\to 0} = 2^{N-1}\alpha \left(1 + e^{\beta \Delta U}\right)^{-1} \; ; \; W^{Star}_{n\to n-1} = \alpha(n-1) \left(1 + e^{\beta \Delta U}\right)^{-1} \quad \text{for } n \geq 1 \, . \tag{4.4}$$

In section A.7 we verify that these transition rates satisfy the *detailed balance* condition (2.26), also for the All-To-All model. This implies that the steady state probabilities follow a Gibbs distribution, and consequently, both the Energy and FI will correspond to those of a Gibbs state, with the hamiltonian H_{star} given in (3.24).

Moving on to the All-to-All model, it is easier to construct the transition rates since there is only one type of eigenstates. Again, using n as the total number of spins up, the energies E_n are given by (3.36), with degeneracy $g_n = \binom{N}{n}$. Therefore, the transition rates become

$$W^{All}_{n\to n+1} = \alpha(N-n) \left(1 + e^{\beta \Delta U}\right)^{-1} \tag{4.5}$$

$$W^{All}_{n\to n-1} = \alpha n \left(1 + e^{\beta \Delta U}\right)^{-1} \, . \tag{4.6}$$

Now we can insert this rates, derived for both systems, into (4.2) to obtain the master equations governing the populations. From here, the problem reduces to solving a system of $N + 1$ differential equations for each system. This task can be easily addressed by implementing a *Python* program that numerically solves the system and returns the solutions $p_n(t)$. This codes are provided and explained in section C.

As an example, we consider the case $N = 5$ for the Star Model, and take the solution for $p_3(t)$. Fixing $\beta = \alpha = 1$, we obtain

$$p_3(t) = 0.0014 + 0.061e^{-0.941t} + 0.024e^{-1.319t} + 1.411e^{-2.001t} - 2.248e^{-3t} + 0.915e^{-4t} \tag{4.7}$$

$$p_3(t \to \infty) \approx 0.0014 \tag{4.8}$$

$$p_3^{Gibbs}(\beta = 1) = \frac{e^{-\varepsilon_3^{Star}}}{\mathcal{Z}_{Star}} = 0.0014 \, , \tag{4.9}$$

where we have used the energy ε_3^{Star} and partition function, both computed using python codes that can be found in section C. As expected, in the limit of long interaction times, the populations approaches the corresponding Gibbs value. This is the consistency check we have been applying throughout the derivations and calculations to ensure that the solutions $p_n(t)$ obtained were correct.

4.2 Energy and Fisher Information during thermalization

Now that we have obtained the solutions of (4.2) for both the Star and All-To-All models, we can compute the time evolution of the energy and the FI.

To describe the energy evolution, we simply compute $E(t) = \text{tr}, [\varrho(t)H]$. Luckily, Lindblad dynamics preserve *diagonality* in the energy eigenbasis, allowing us to simplify this expression to

$$E(t) = \sum_n E_n \, p_n(t) \, , \tag{4.10}$$

which is straightforward to plot now that we have both $p_n(t)$ and E_n.

On the other hand, in order to plot $\mathcal{F}_\beta(t)$ we need to compute $\partial_\beta p_n(t)$. This can be challenging, given that $p_n(t)$ were obtained numerically for a fixed value of $\beta = 1$. A direct analytical derivative with respect to β would be impractical, so we instead use the numerical definition of

a derivative to approach the problem. As we mentioned, our python programs, introduced in C, are capable of computing numerical solutions for p_n for a fixed value β. Therefore, using a *very small* step h we can find

$$\partial_\beta p_n(t) \approx \frac{p_n(\beta+h,t) - p_n(\beta,t)}{h} \ . \tag{4.11}$$

For the plots shown in Figure 4.1, after different trials, we selected $h = 0.0008$ and $\beta = 1$.

Now, we already have all the ingredients we need to visualize how this two quantities behave during this thermalization process. For a single set of measurements, we can adapt the FI defined in (2.2) as

$$\mathcal{F}_\beta(t) = \sum_n \frac{(\partial_\beta\, p_n(t))^2}{p_n(t)} \ . \tag{4.12}$$

Thus, introducing (4.11) and the obtained $p_n(t)$ in (4.12), and using (4.10), we can compute the following figures.

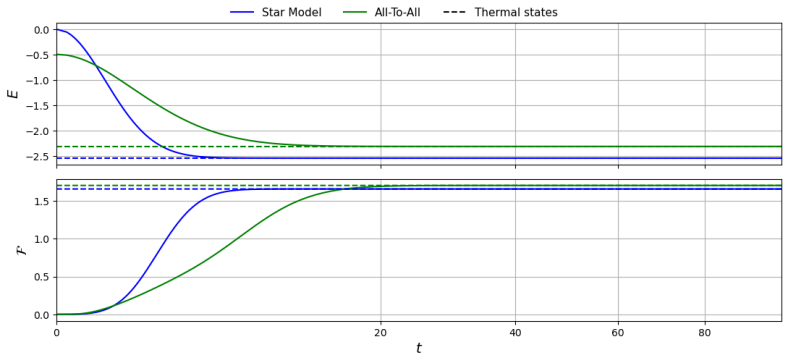

(a) $N = 3$

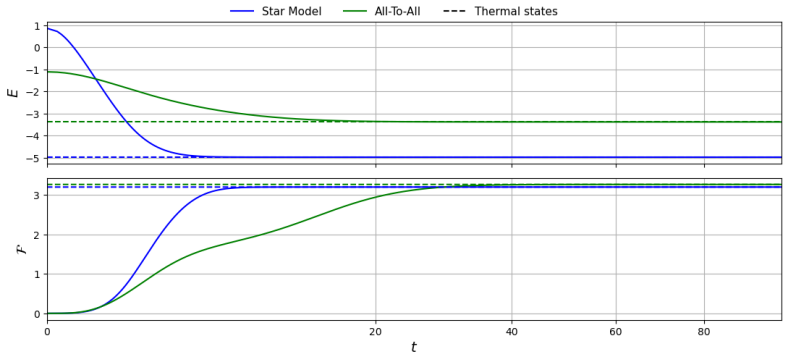

(b) $N = 5$

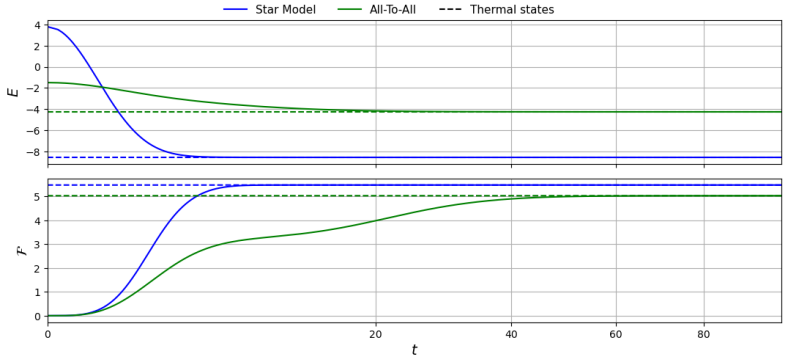

(c) $N = 7$

Figure 4.1: Energy and FI over time during thermalization, using $\beta = \alpha = 1$, $h = 0.0008$ and initial states $p_n = 1/(N+1)$.

We can observe several important features in this figure. First, as seen in section 3, the All-to-All model provides a slight advantage in equilibrium thermometry for $N \leq 5$. However, its thermalization times are considerably longer than those of the Star Model—particularly for the Fisher Information, which increases much more rapidly with N in the All-to-All case, while the energy thermalization times remain nearly constant.

This difference can be understood by noting that, although the expected value of the energy reaches equilibrium relatively quickly, the Fisher Information does not necessarily do so at the same time. The energy, being a first-moment observable, depends linearly on the population distribution and typically relaxes under the dominant decay modes of the dynamics. In contrast, the Fisher Information is a nonlinear functional that captures the sensitivity of the populations to temperature, making it much more responsive to small perturbations. As a result, it converges more slowly and its thermalization times grow significantly with system size. In the following section, we will examine in detail how these thermalization times behave with increasing N for the Star Model.

4.3 Optimization trade-offs

To understand how the thermalization timescales behave as the system size increases, we analyze the decay rates obtained from the solutions to the master equation. In particular, by studying how the dominant (i.e., slowest) decay rate depends on N, we can have an idea of the trade-off between enhanced Fisher Information and slower thermalization.

These decay rates correspond to the eigenvalues of the generator that governs the dynamics. Since the populations evolve according to the Lindblad master equation (2.19), our decay rates are given by the eigenvalues of the associated Lindbladian (2.20).

As previously discussed, these solutions were obtained using Python scripts (detailed in Section C). In the figure below, we plot the quantity $1/|\lambda_1|$ as a function of N, where λ_1 denotes the smallest non-zero eigenvalue in absolute value. The populations evolve as

$$p_n(t) = \sum_i A_i e^{\lambda_i t}, \tag{4.13}$$

where all eigenvalues $\lambda_i \leq 0$. The coefficient A_0, associated with the zero eigenvalue $\lambda_0 = 0$, determines the asymptotic (equilibrium) population $p_n(t \to \infty)$. Thus, the inverse of $|\lambda_1|$ provides a useful estimate of the thermalization timescale, as terms with $|\lambda_i| \gg |\lambda_1|$ decay much faster and quickly become negligible.

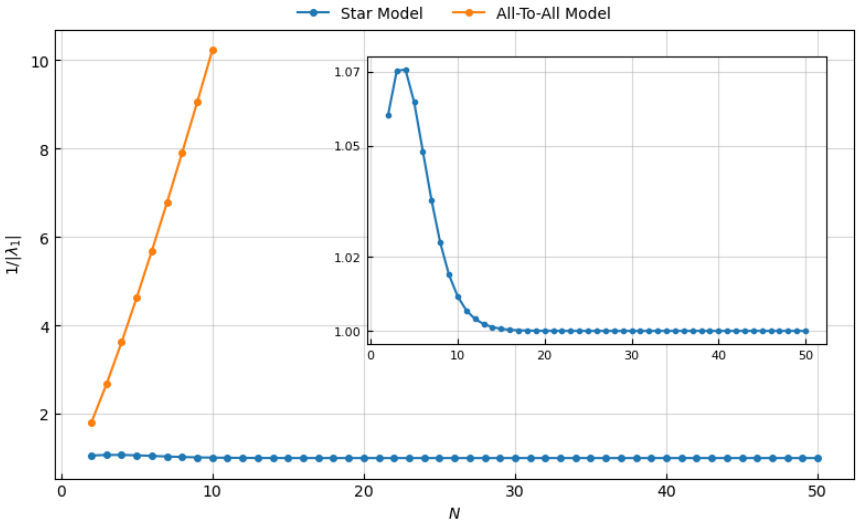

Figure 4.2: Scaling of the thermalization timescale $1/|\lambda_1|$ with system size N. The main panel compares the All-to-All model (for $N \in [2, 10]$) with the Star Model (for $N \in [2, 50]$). The inset highlights the behavior of the Star Model in greater detail.

As expected, the All-to-All model exhibits a rapid increase in the thermalization timescale with growing N. In contrast, the Star Model remains nearly constant beyond $N \geq 17$, and even shows longer timescales for small system sizes. This difference can be attributed to the nature of interactions in each model: while the All-to-All configuration scales its connectivity with N, the Star Model maintains a central-spin symmetry that remains relatively unchanged as more peripheral spins are added.

As we have just discussed, optimizing the value of the FI by increasing the system size N comes at the cost of longer thermalization times for the All-To-All model [17]. This reveals a clear trade-off; while larger N enhances sensitivity, longer interaction times may introduce external noise and degrade the probe's performance. With the results obtained so far, we can conclude that the Star Model exhibits more favorable features than the All-to-All configuration, including shorter thermalization times and convergence toward the optimal FI bound for large N.

Focusing now on the Star Model, let us consider a practical scenario where measurements must be performed during the transient (non-equilibrium) regime. Suppose there exists a fixed total estimation time $\mathcal{T}$, constrained by experimental limitations. In this case, the protocol must be separeted in an optimal number $\mathcal{N} = \mathcal{T}/t$ of steps, composed of preparation, evolution, and measurement. The Cramér-Rao bound (CRB) then reads:

$$\Delta T \geq \frac{1}{\sqrt{\mathcal{N}\mathcal{F}(t)}} = \frac{1}{\sqrt{(\mathcal{T}/t)\mathcal{F}(t)}} \ . \tag{4.14}$$

This introduces a new figure of merit to be maximized: $\eta_{\mathcal{T}}(t) := \mathcal{F}(t)/t$, which quantifies the information gained per unit time. Importantly, the time t that maximizes $\eta_{\mathcal{T}}(t)$—the optimal interrogation time—does not necessarily coincide with the thermalization time of the FI.

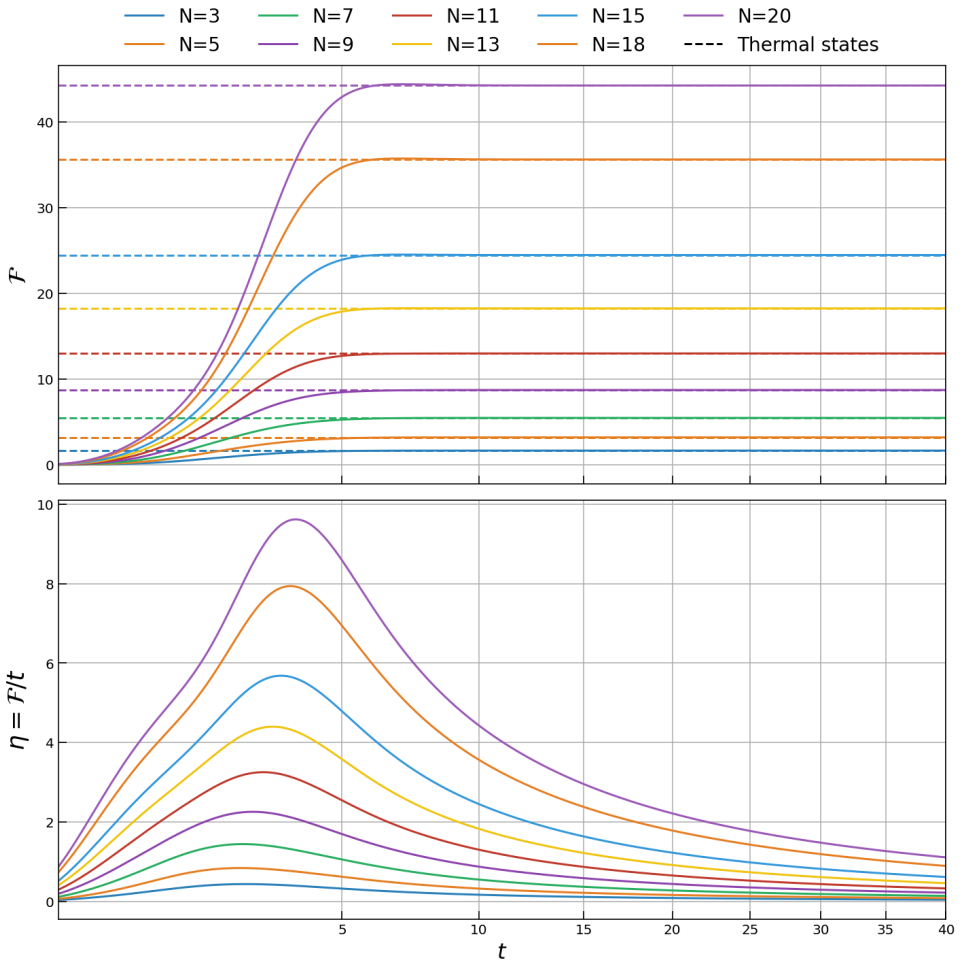

Figure 4.3: Evolution in time of the Fisher Information and $\eta_{\mathcal{T}}(t)$, for the Star Model and different values of N.

In Figure 4.3, we show the evolution of both the Fisher Information (FI) and the quantity $\eta_{\mathcal{T}}(t)$, illustrating that the optimal time for $\eta_{\mathcal{T}}$ is reached slightly before the FI attains its equilibrium value. Therefore, if the goal of an experiment is to maximize estimation precision while minimizing interaction time — or if the interaction time is constrained to be $\mathcal{T}$ — optimizing $\eta_{\mathcal{T}}$ provides the best configuration for measurement.

Furthermore, we observe in Figure 4.3 a slight increase in the thermalization time of the FI as N increases. At first sight, this may appear to contradict Figure 4.2, which suggests that the dominant decay rate λ_1 becomes nearly constant for large N. One possible explanation is that Figure 4.2 only considers the smallest non-zero eigenvalue, while other decay modes may still be subtly affected by increasing N. Another possibility is that, as previously discussed, the FI is a nonlinear functional that captures the sensitivity of the populations to temperature changes, which makes it more sensitive to small variations in the distribution. Lastly, it is worth considering whether the initial state of the probe plays a role in this behavior. To investigate this, we construct Figure 4.4, comparing the thermalization process starting from an equiprobable state $p_n(0) = 1/(N+1)$ versus a ground state initialization $p_1(0) = 1$ (the latter being the state in which only the central spin is up in the Star Model).

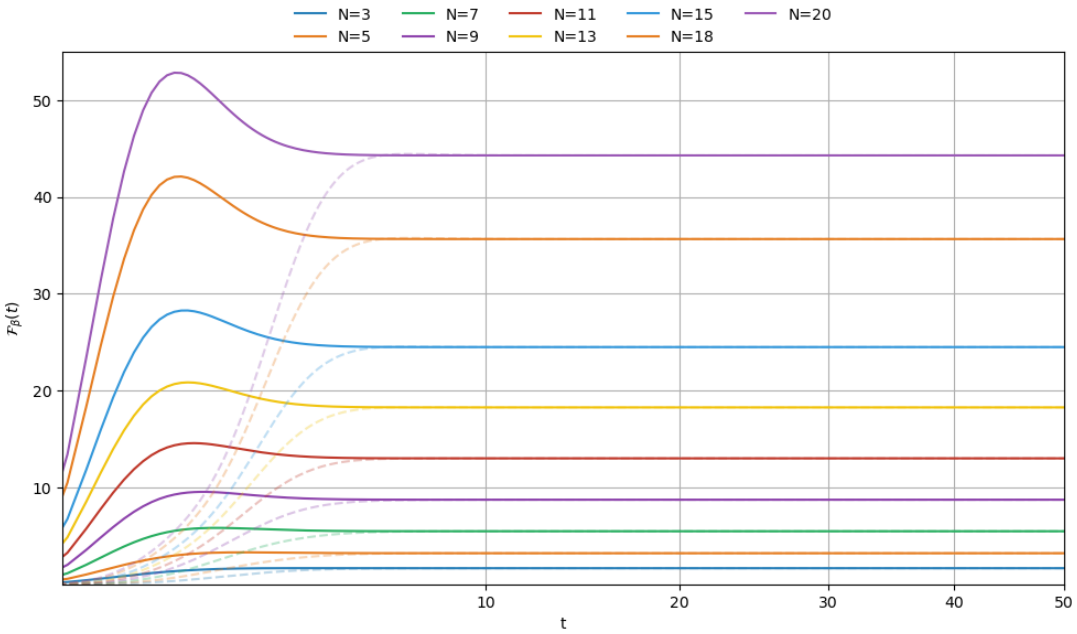

Figure 4.4: Evolution over time of the Fisher Information for two different initial states. Solid lines represent the ground state initialization, while dashed lines correspond to the equiprobable state.

We observe that, although the final thermalization point is nearly identical, initializing the system in its ground state leads to higher FI values during the transient regime. This may result from the fact that concentrating all population in a single energy level increases the sensitivity to small temperature variations. Alternatively, it could be that the initially populated levels in the equiprobable case are less responsive to temperature shifts compared to those near the ground state. This behavior could be exploited in scenarios where measurements must be performed before the system reaches equilibrium.

Chapter 5

Conclusions

5.1 Summary

In this work, we have developed a comprehensive study of quantum thermometry, focusing on both equilibrium and dynamical regimes. After building the theoretical foundation and optimal bounds, we evaluated two physically motivated models: the Star and the All-to-All configurations. These models appeared in recent works after optimizing all possible two-body spin network configurations. The analysis showed that the Star Model approaches the optimal bound at large system sizes, while the All-to-All Model performs better for small probes, despite its longer thermalization times.

We then extended our analysis to dynamical quantum thermometry, to develop new results in the field by simulating thermalization via Lindblad master equations. We observed that energy reaches equilibrium relatively quickly, while the QFI — being more sensitive to fine-grained features of the population distribution — converges more slowly. This highlights a trade-off between thermometric sensitivity and thermalization time that becomes more pronounced with increasing system size.

Overall, this work combines analytical insights with numerical simulations to clarify how structure and dynamics affect the performance of quantum thermometers. These findings highlight practical limitations in out-of-equilibrium thermometry and can inform the design of efficient quantum sensors for applications in low-temperature physics, quantum heat engines, and non-equilibrium thermodynamics.

5.2 Outlook (or future and actual work)

Recent developments in quantum thermometry suggest several promising directions for extending this work. One is exploring optimal finite-time estimation strategies using local controls or coarse-grained measurements, which may enhance practicality without sacrificing precision. Incorporating adaptive schemes or periodically driven dynamics could also improve sensitivity in the transient regime. On the experimental side, implementing spin-network thermometers in platforms like trapped ions or superconducting qubits is becoming increasingly feasible. Finally, integrating thermometric tasks with quantum heat engines — a direction explored by Perarnau-Llobet and collaborators — offers a path toward multifunctional quantum devices that combine sensing and thermodynamic processing.

Appendix A

Detailed derivations

A.1 ∂_T of the Gibbs state

Using $\hat{\varrho}(\beta) = \frac{e^{-\beta H}}{Z}$ with $Z = \mathrm{tr}(e^{-\beta H})$

$$\frac{\partial \varrho}{\partial T} = -\frac{1}{T^2}\frac{\partial \varrho}{\partial \beta} \tag{A.1}$$

$$\rightarrow \frac{\partial \varrho}{\partial \beta} = \frac{-He^{-\beta H}Z + e^{-\beta H}\cdot \mathrm{tr}(He^{-\beta H})}{Z^2} = \frac{1}{Z}(-He^{-\beta H} + \langle H\rangle e^{-\beta H}) \tag{A.2}$$

$$= \varrho(\langle H\rangle - H) \tag{A.3}$$

$$\frac{\partial \varrho}{\partial T} = \frac{1}{T^2}\varrho(H - \langle H\rangle) \tag{A.4}$$

A.2 SLD of the Gibbs state

We have from (A.1) and from the definition of the SLD in (2.6), that

$$\frac{\partial \varrho}{\partial T} = \frac{1}{T^2}\varrho(H - \langle H\rangle) \tag{A.5}$$

$$\frac{\partial \varrho}{\partial T} = \frac{1}{2}\{L_T, \varrho\} \tag{A.6}$$

So to determine L_T we try an ansatz: $L_T = \alpha(H - \langle H\rangle)$ where α is some constant, and we plug this ansatz into the SLD definition:

$$\frac{1}{2}\{\hat{L}_T, \hat{\varrho}\} = \frac{\alpha}{2}\{H - \langle H\rangle, \hat{\varrho}\} = \alpha(H\hat{\varrho} - \langle H\rangle\hat{\varrho}) \tag{A.7}$$

Where we have used that $\langle H\rangle$ is a scalar so it commutes with everything, and $\hat{\varrho}$ and H also commute since $\hat{\varrho}$ can be understood as an exponential map of H, and we know that $[\hat{H}, f(\hat{H})] = 0$. Now comparing (A.5) and (A.6) we can see that $\alpha = 1/T^2$, thus the SLD

$$\hat{L}_T = \frac{1}{T^2}(\hat{H} - \langle H\rangle) \tag{A.8}$$

A.3 Rewriting the uncertainty relation 2.15

The 'potential-of-mean-force' approach consists in adopting the modified partition function

$$\mathcal{Z}_p := \frac{\mathrm{Tr}\, e^{-\beta(\hat{H}_p + \hat{H}_S + \hat{H}_I)}}{\mathrm{Tr}\, e^{-\beta \hat{H}_S}} \tag{A.9}$$

for the probe. And its internal energy becomes

$$-\partial_\beta \log \mathcal{Z}_p = \langle \hat{H}\rangle - \langle \hat{H}_S\rangle = \langle \hat{E}_p^*\rangle, \tag{A.10}$$

with

$$\hat{E}_p^* := \partial_\beta \left[\beta \hat{H}_p^*(\beta)\right], \tag{A.11}$$

$$\hat{H}_p^*(\beta) := -\beta^{-1} \log \frac{\mathrm{Tr}_S \exp\left[-\beta(\hat{H}_p + \hat{H}_S + \hat{H}_I)\right]}{\mathrm{Tr}\exp\left(-\beta \hat{H}_S\right)}, \tag{A.12}$$

so $\hat{\varrho}_P = \mathcal{Z}_p^{-1} e^{-\beta \hat{H}_p^*}$. The variance of the modified energy operator $\hat{E}_p^*$, can be separated as the sum of two contributions

$$(\Delta \hat{E}_p^*)^2 = Q_\alpha(\hat{\varrho}_p, \hat{E}_p^*) + C_\alpha(\hat{\varrho}_p, \hat{E}_p^*), \tag{A.13}$$

meaning its 'quantum' and 'classical' parts, respectively. In particular,

$$Q_\alpha(\hat{\varrho}, \hat{A}) := -\frac{1}{2}\mathrm{Tr}\left(\left[\hat{A}, \hat{\varrho}^\alpha\right]\left[\hat{A}, \hat{\varrho}^{1-\alpha}\right]\right) \tag{A.14}$$

is known as the Wigner–Yanase skew information, where $\alpha \in (0,1)$. Then, the decomposition of $(\Delta \hat{A})^2$ into quantum and classical part is not unique. The relation between $(\Delta \hat{E}_p^*)^2$ and $\mathcal{F}(\beta, \hat{E}_p^*)$ can be established by noticing that

$$C(\hat{\varrho}P, \hat{E}_P^*) := \int_0^1 d\alpha\, C\alpha(\hat{\varrho}_P, \hat{E}_P^*) \geq \mathcal{F}(\beta, \hat{E}_P^*) \tag{A.15}$$

thus, from the Cramér–Rao bound, $(\Delta\beta)^2 \geq C(\hat{\varrho}P, \hat{E}_P^*)^{-1} = \left[(\Delta \hat{E}_P^*)^2 - Q\alpha(\hat{\varrho}_P, \hat{E}_P^*)\right]^{-1}$, where $Q(\cdot,\cdot)$ is defined like $C(\cdot,\cdot)$ in equation (A.15). As a result we obtain

$$\Delta\beta \geq \frac{1}{\sqrt{(\Delta \hat{E}P^*)^2 - Q\alpha(\hat{\varrho}_P, \hat{E}_P^*)}} \geq \frac{1}{\Delta \hat{E}_P^*}. \tag{A.16}$$

what is a generalization of (2.15), taking into account the strong probe-system coupling.

A.4 Classical Fisher Information of a Gibbs state

Imagine we measure $\rho(T)$ and obtain a probability distribution $p(T)$. Then the classical Fisher F info is given by:

$$\mathcal{F}(T) = \sum_j \frac{(\partial_T p_j(T))^2}{p_j(T)} \tag{A.17}$$

Assume a Hamiltonian $H = \sum_j e_j |j\rangle\langle j|$ and that $\rho(T)$ is given by a thermal state:

$$\rho(T) = \frac{e^{-\beta H}}{\mathrm{Tr}(e^{-\beta H})}, \tag{A.18}$$

We can write $\rho(T) = \sum_j p_j |j\rangle\langle j|$, where the $p_j(T)$ follow a Gibbs distribution:

$$p_j(T) = \frac{e^{-\beta e_j}}{\mathcal{Z}} \tag{A.19}$$

where $\mathcal{Z} = \mathrm{Tr}(e^{-\beta H})$.

To obtain the expression for the Fisher Information of this Gibbs state we should start finding $\partial_T p_j(T)$:

$$\partial_T p_j(T) = \frac{\partial}{\partial T}(\frac{e^{-\beta\epsilon_j}}{\mathcal{Z}}) = -\frac{1}{T^2}\frac{\partial}{\partial\beta}(\frac{e^{-\beta\epsilon_j}}{\mathcal{Z}}) \tag{A.20}$$

$$= \frac{1}{T^2}\frac{\epsilon_j e^{-\beta\epsilon_j}\mathcal{Z} + e^{-\beta\epsilon_j}\partial_\beta\mathcal{Z}}{\mathcal{Z}^2} \tag{A.21}$$

$$= \frac{1}{T^2}\frac{e^{-\beta e_j}}{\mathcal{Z}}(\epsilon_j + \frac{\partial_\beta\mathcal{Z}}{\mathcal{Z}}) \tag{A.22}$$

$$= \frac{1}{T^2}\, p_j(\epsilon_j + \partial_\beta \ln\mathcal{Z}) \tag{A.23}$$

$$= \frac{1}{T^2}\,(p_j\epsilon_j - p_j\langle H\rangle) \tag{A.24}$$

In the last step we have used the relation $\partial_\beta \ln\mathcal{Z} = -\langle H\rangle$. We can introduce this result in (A.17) and obtain the following relation:

$$\mathcal{F}(T) = \sum_j \frac{(\partial_T p_j)^2}{p_j} = \frac{1}{T^4}\sum_j \frac{(p_j\langle H\rangle - p_j\epsilon_j)^2}{p_j} \tag{A.25}$$

$$= \frac{1}{T^4}\sum_j \left(p_j\langle H\rangle^2 + p_j\epsilon_j^2 - 2\langle H\rangle p_j\epsilon_j\right) \tag{A.26}$$

$$= \frac{1}{T^4}\left(\langle H\rangle^2\sum_j p_j \;+ \sum_j p_j\epsilon_j^2 - 2\langle H\rangle\sum_j p_j\epsilon_j\right) \tag{A.27}$$

$$= \frac{1}{T^4}\left(\langle H\rangle^2 + \langle H^2\rangle - 2\langle H\rangle^2\right) = \frac{\langle H^2\rangle - \langle H\rangle^2}{T^4} = \frac{(\Delta H)^2}{T^4} \tag{A.28}$$

As expected, it is the same exact result that we had for the QFI in (2.13). Notice that this result would be different if we do the calculous with respect the inverse temperature β, as we would not obtain the factor $1/T^4$ (with $k_B = 1$).

A.5 Optimal gap

We have that

$$x^* = 2\left(1 + \frac{\langle H\rangle}{T}\right), \tag{A.29}$$

so we need to find $\langle H\rangle$. For a general 2-level system, with N_0 particles in the ground state ($\epsilon_1 = 0$) and $N - N_0$ on the excited one ($\epsilon_2 = \Omega$), the partition function is $\mathcal{Z} = N_0 + (N - N_0)e^{-\frac{\Omega}{T}}$, thus:

$$\langle H\rangle = T^2\partial_T \ln\mathcal{Z} = T^2\frac{\partial_T\mathcal{Z}}{\mathcal{Z}} = \frac{(N - N_0)\Omega e^{-\frac{\Omega}{T}}}{N_0 + (N - N_0)e^{-\frac{\Omega}{T}}}\,. \tag{A.30}$$

We can now introduce this result into (A.29) and obtain

$$x^* = 2(1 + \langle H\rangle/T) = 2\left(1 + \frac{(N - N_0)x^*e^{-x^*}}{N_0 + (N - N_0)e^{-x^*}}\right) \tag{A.31}$$

$$(x^* - 2)(N_0 + (N - N_0)e^{-x^*}) = 2(N - N_0)x^*e^{-x^*} \tag{A.32}$$

$$(x^* - 2)N_0 + e^{-x^*}(x^* - 2)(N - N_0) - 2(N - N_0)x^*e^{-x^*} = 0 \tag{A.33}$$

$$e^{-x^*}\,(x^* - 2 - 2x^*) = \frac{(x^* - 2)N_0}{N - N_0} \tag{A.34}$$

$$e^{x^*} = \frac{N - N_0}{N_0}\frac{x^* + 2}{x^* - 2} \tag{A.35}$$

which is the equation that we will use to find the value of x^* for different values of N.

A.6 Partition function $\mathcal{Z}$ for the Star Model

We can separate by the value of the first spin σ_1^z in Z_+ and Z_-

$$Z_+ = \sum_{i=1} g_i e^{-E_i\beta} = \sum_{\vec{\sigma}^z} e^{-\beta H_{star}[\vec{\sigma},\sigma_1^z=+1]} = e^{-\beta a} \sum_{\vec{\sigma}^z} e^{-2\beta b \sum_{i=2}^N \sigma_i^z} \tag{A.36}$$

$$= e^{-\beta a} \prod_{i=2}^{N} \sum_{\sigma_i^z=\pm 1} e^{-2\beta b \sigma_i^z} = e^{-\beta a}(e^{-2\beta b} + e^{-2\beta b})^{N-1} \tag{A.37}$$

$$= 2^{N-1} e^{-\beta a} \cosh(2\beta b)^{N-1} \tag{A.38}$$

$$Z_- = \sum_{i=1} g_i e^{-E_i\beta} = 2^{N-1} e^{\beta a} \tag{A.39}$$

$$Z_{\text{star}} = Z_+ + Z_- = 2^{N-1}(e^{-\beta a} \cosh(2\beta b)^{N-1} + e^{\beta a}) \tag{A.40}$$

A.7 Detailed balance check

For systems with degeneracy in the different energy levels, we have to add a factor in 2.26 that gives us

$$g_n W_{n\to m} \exp(-\beta\varepsilon_n) = g_m W_{m\to n} \exp(-\beta\varepsilon_m)\,. \tag{A.41}$$

Starting with the Star Model, we check first the particular rates for $n = 0$:

$$g_0 W_{0\to 1} \exp(-\beta\varepsilon_0) = g_1 W_{1\to 0} \exp(-\beta\varepsilon_1) \tag{A.42}$$

$$2^{N-1}\alpha(1 + e^{\beta\Delta U_{1\to 0}})^{-1} e^{-\beta\varepsilon_0} = 1 \cdot 2^{N-1}\alpha(1 + e^{\beta\Delta U_{0\to 1}})^{-1} e^{-\beta\varepsilon_1} \tag{A.43}$$

$$\frac{1 + e^{\beta\Delta U_{0\to 1}}}{1 + e^{\beta\Delta U_{1\to 0}}} = e^{\beta(\varepsilon_0 - \varepsilon_1)} \tag{A.44}$$

$$\frac{1 + e^{\beta\Delta U_{0\to 1}}}{1 + e^{-\beta\Delta U_{0\to 1}}} = e^{\beta\Delta U_{0\to 1}} \tag{A.45}$$

$$e^{\beta\Delta U_{0\to 1}} = e^{\beta\Delta U_{0\to 1}} \quad \checkmark \tag{A.46}$$

Where we have used $\Delta U_{1\to 0} = -\Delta U_{0\to 1}$. For a general $n \geq 1$ we got

$$g_n W_{n\to n+1} \exp(-\beta\varepsilon_n) = g_{n+1} W_{n+1\to n} \exp(-\beta\varepsilon_{n+1}) \tag{A.47}$$

$$\binom{N-1}{n-1}\alpha(N-n)\left(1 + e^{\beta\Delta U_{n+1\to n}}\right)^{-1} e^{-\beta\varepsilon_n} = \binom{N-1}{n}\alpha n\left(1 + e^{\beta\Delta U_{n\to n+1}}\right)^{-1} e^{-\beta\varepsilon_{n+1}} \tag{A.48}$$

$$\frac{N-n}{n}\,\frac{1 + e^{\beta\Delta U_{n\to n+1}}}{1 + e^{\beta\Delta U_{n+1\to n}}} = \frac{\binom{N-1}{n}}{\binom{N-1}{n-1}} e^{\beta\Delta U_{n\to n+1}} \tag{A.49}$$

We know that the exponential terms coincide, as we just did for $n = 0$. Therefore, checking that

$$\frac{\binom{N-1}{n}}{\binom{N-1}{n-1}} = \frac{\frac{(N-1)!}{n!(N-1-n)!}}{\frac{(N-1)!}{(n-1)!(N-n)!}} = \frac{(n-1)!(N-n)!}{n!(N-1-n)!} = \frac{(n-1)!}{n\cdot(n-1)!} \cdot \frac{(N-n)\cdot(N-1-n)!}{(N-1-n)!} \tag{A.50}$$

$$= \frac{N-n}{n} \quad \checkmark \tag{A.51}$$

we can say that detailed balance is satisfied for the calculated rates of the Star Model.

Identically for the All-to-All model. We just have to replace the terms with $n-1$ by just n to easily see that detailed balance is also satisfied for the rates in (4.5) and (4.6).

Appendix B

All-to-All model data

Table B.1: All-to-All model data

N	Z	C_{max}	J_{opt}
2	$e^{3\beta J} + 3e^{-\beta J}$	1.023	0.7112
3	$e^{6\beta J} + 3e^{-2\beta J} + 4$	1.706	0.4960
4	$5e^{2\beta J} + e^{10\beta J} + 10e^{-2\beta J}$	2.461	0.3769
5	$6e^{5\beta J} + e^{15\beta J} + 10e^{-3\beta J} + 15e^{-\beta J}$	3.274	0.3019
6	$21e^{\beta J} + 7e^{9\beta J} + e^{21\beta J} + 35e^{-3\beta J}$	4.135	0.2506
7	$28e^{4\beta J} + 8e^{14\beta J} + e^{28\beta J} + 35e^{-4\beta J} + 56e^{-2\beta J}$	5.034	0.2135
8	$36e^{8\beta J} + 9e^{20\beta J} + e^{36\beta J} + 126e^{-4\beta J} + 84$	5.968	0.1856
9	$120e^{3\beta J} + 45e^{13\beta J} + 10e^{27\beta J} + e^{45\beta J} + 126e^{-5\beta J} + 210e^{-3\beta J}$	6.931	0.1638
10	$165e^{7\beta J} + 55e^{19\beta J} + 11e^{35\beta J} + e^{55\beta J} + 462e^{-5\beta J} + 330e^{-\beta J}$	7.920	0.1464

Appendix C

Python Codes

In this section we will introduce the python codes used to solve some aspects of this work. We will only explain in detail the code used to solve the rate equations, since is the only code with mathematical impact in the calculations of this work.
The codes used for plotting the different figures are:

- `FisherInformation(T).py` — Plotting of Figure 3.1
- `C(N).py` — Plotting of Figure 3.2
- `Thermalization E and F.py` — Simulating the thermalization process of the Energy and Fisher Information and plotting of Figure 4.1
- `Fisher and Eta N20.py` — Simulating the thermalization process of both Fisher Information and $\eta_{\mathcal{T}}$ in a of $N = 20$ Star Model, and plotting Figure 4.3.
- `Decay Rates.py` — Plotting Figure 4.2.
- `Thermalization Fisher Json.py` — Plotting Figure 4.4.

Other codes used as a support for plots or second-rate calculations:

- `Find X opt.py` — Calculation of optimal gaps through equation 3.5.
- `Energies and Partition Functions.py` — Finding Energies and Partition functions for different values of N for both Star and All-To-All model
- `Gibbs Probabilities.py` — Calculation of the Gibbs populations for both Star and All-To-All models, used to plot the thermal states in Figure 4.1.

Now focusing on the Python script that solves the Pauli master equation (2.24) for the population dynamics of the Star Model. The main components of the code are:

- **Energy function `U(N, n)`:** Defines the internal energy of the Star Model at excitation level n, based on effective parameters a and b taken from lists for each system size N [3].
- **Fermi-like function `f(x, beta)`:** Implements the transition probability for a process with energy change x at inverse temperature β, using the expression $f(x, \beta) = \frac{1}{1+e^{\beta x}}$.
- **Function `transition_matrix(N, beta)`:** Constructs the rate matrix M governing the dynamics via the Pauli master equation:

$$\frac{d\vec{p}}{dt} = M\vec{p} \tag{C.1}$$

  Each element $M_{m,n}$ represents the rate of transition from state n to m, and the matrix is built to ensure probability conservation (i.e., columns sum to zero).

- **Time evolution:** The solution $\vec{p}(t)$ at time t is computed via matrix exponentiation using $\vec{p}(t) = e^{Mt}\vec{p}(0)$, where $\vec{p}(0)$ is the initial state (that can be adjusted in lines 53-56).
- **Spectral decomposition:** The code diagonalizes the matrix M to express each component $p_n(t)$ as a sum of exponentials:

$$p_n(t) = \sum_k A_{n,k}\, e^{\lambda_k t} \tag{C.2}$$

  where λ_k are the eigenvalues and $A_{n,k}$ are coefficients determined by the eigenvectors and the initial state. This decomposition reveals how each mode contributes to thermalization.

The script outputs a .json file with the full analytical form of $p_n(t)$, giving insight into how each population evolves toward equilibrium.

```
1  import numpy as np
2  from scipy.linalg import expm, eig, inv
3  import json
4
5  # Predefined values
6  a_values = [-0.711, 0.000, 0.894, 2.015, 3.398, 5.070, 7.052, 9.358,
       11.998, 14.977,
7              18.297, 21.960, 25.967, 30.318, 35.013, 40.053, 45.438,
                   51.168, 57.243, 63.664,
8              70.431, 77.543, 85.001, 92.805, 100.956, 109.452, 118.294,
                   127.483, 137.018, 146.899,
9              157.127, 167.701, 178.621, 189.887, 201.500, 213.460,
                   225.766, 238.418, 251.417, 264.762,
10             278.453, 292.492, 306.876, 321.607, 336.685, 352.109,
                   367.879, 383.996, 400.460]
11
12 b_values = [0.711, 0.797, 0.894, 1.007, 1.133, 1.267, 1.410, 1.560,
       1.714, 1.872,
13             2.033, 2.196, 2.361, 2.527, 2.693, 2.861, 3.029, 3.198,
                   3.367, 3.537,
14             3.707, 3.877, 4.048, 4.218, 4.389, 4.560, 4.732, 4.903,
                   5.075, 5.246,
15             5.418, 5.590, 5.762, 5.934, 6.106, 6.278, 6.450, 6.623,
                   6.795, 6.967,
16             7.140, 7.312, 7.485, 7.657, 7.830, 8.002, 8.175, 8.348,
                   8.520]
17
18 # Helper functions
19 def U(N, n, a, b):
20     return -a if n == 0 else a + 2 * b * (2 * (n - 1) - (N - 1))
21
22 def f(x, beta):
23     return 1 / (1 + np.exp(beta * x))
24
25 def transition_matrix(N, beta, a, b):
26     M = np.zeros((N + 1, N + 1))
27     for n in range(N + 1):
28         if n == 0:
29             delta_U = U(N, n + 1, a, b) - U(N, n, a, b)
30             rate_up = f(delta_U, beta)
31             M[n, n] -= rate_up
32             M[n + 1, n] += rate_up
33         if n < N and n != 0:
34             delta_U = U(N, n + 1, a, b) - U(N, n, a, b)
35             rate_up = (N - n) * f(delta_U, beta)
```

```
            M[n, n] -= rate_up
            M[n + 1, n] += rate_up
        if n > 0:
            delta_U = U(N, n - 1, a, b) - U(N, n, a, b)
            rate_down = (2 ** (N - 1) if n == 1 else (n - 1)) * f(
                delta_U, beta)
            M[n, n] -= rate_down
            M[n - 1, n] += rate_down
    return M

# Main computation loop
target_Ns = [3, 5, 7, 9, 11, 13, 15, 18, 20]
beta = 1
prob_functions = {}

for N in target_Ns:
    a = a_values[N - 2]
    b = b_values[N - 2]
    p0 = np.full(N + 1, 0)
    #excited = int(N/2)
    p0[0] = 1
    #p0=np.full(N+1, 1/(N+1))
    M = transition_matrix(N, beta, a, b)
    eigvals, eigvecs = eig(M)
    V_inv = inv(eigvecs)
    coeffs = V_inv @ p0

    prob_functions[N] = {}
    for n in range(N + 1):
        terms = []
        for k in range(N + 1):
            amplitude = eigvecs[n, k] * coeffs[k]
            if np.abs(amplitude) > 1e-6:
                real_part = np.real(amplitude)
                decay = np.real(eigvals[k])
                terms.append(f"{real_part:.8f} * np.exp({decay:.8f} * t)
                    ")
        prob_functions[N][n] = " + ".join(terms)

# Save as JSON
import os
output_path = r"C:\Users\alber\OneDrive\Escritorio\TFG\JSON\
    prob_ground_beta1.json"
with open(output_path, "w") as f:
    json.dump(prob_functions, f, indent=2)

output_path
```

Listing C.1: Python script solving the master equation for the Star Model.

For the All-To-All model we can use the same script just replacing some functions. First, the energy must be the one defined by (3.36), using the J values given in B.1. Then we have to replace the `transition_matrix(N, beta)` function by a simpler definition. Just to adapt it to the transition rates we have in (4.5) and (4.6).

Then the first part of the code becomes:

```
J_values = [0.7112, 0.496, 0.3769, 0.3019, 0.2506, 0.2135, 0.1856,
    0.1638, 0.1464]

def U(N,n):
    return J*(-N*(N+1)*0.5 + 2*(n+1)*(N-n))

def f(x, beta):
    return 1 / (1 + np.exp(beta * x))

def transition_matrix(N, beta):
    M = np.zeros((N+1, N+1))

    for n in range(N+1):
        # Transitions from n to n+1
        if n < N:
            delta_U = U(N,n+1) - U(N,n)
            rate_up = (N - n) * f(delta_U, beta)
            M[n, n] -= rate_up
            M[n+1, n] += rate_up

        # Transitions from n to n-1
        if n > 0:
            delta_U = U(N,n-1) - U(N,n)
            rate_down = n * f(delta_U, beta)
            M[n, n] -= rate_down
            M[n-1, n] += rate_down

    return M
```

Listing C.2: Functions defined for the All-To-All model in order to find the analytical solutions for $p_n(t)$

References

[1] Mohammad Mehboudi, Anna Sanpera, and Luis A. Correa. "Thermometry in the quantum regime: Recent theoretical progress". In: *J. Phys. A: Math. Theor.* 52.30 (2019), p. 303001. DOI: 10.1088/1751-8121/ab2828. arXiv: 1811.03988 [quant-ph].

[2] Luis A. Correa, Mohammad Mehboudi, Gerardo Adesso, and Anna Sanpera. "Individual quantum probes for optimal thermometry". In: *Phys. Rev. Lett.* 114.22 (2015), p. 220405. DOI: 10.1103/PhysRevLett.114.220405. arXiv: 1411.2437 [quant-ph].

[3] Paolo Abiuso, Paolo Andrea Erdman, Michael Ronen, Frank Noé, Géraldine Haack, and Martí Perarnau-Llobet. "Optimal thermometers with spin networks". In: *Quantum Science and Technology* 6.2 (2021), p. 024006. DOI: 10.1088/2058-9565/ad37d3. URL: https://iopscience.iop.org/article/10.1088/2058-9565/ad37d3.

[4] Felix Binder, Luis A. Correa, Christian Gogolin, Janet Anders, and Gerardo Adesso, eds. *Thermodynamics in the Quantum Regime*. Fundamental Theories of Physics. Springer, 2018. ISBN: 978-3-319-99046-0. DOI: 10.1007/978-3-319-99046-0. URL: https://link.springer.com/book/10.1007/978-3-319-99046-0.

[5] A. S. Holevo. *Probabilistic and Statistical Aspects of Quantum Theory*. Vol. 1. Springer Science & Business Media, 2011. DOI: 10.1007/978-88-7642-378-9. URL: https://doi.org/10.1007/978-88-7642-378-9.

[6] Karl Kraus. *States, Effects, and Operations: Fundamental Notions of Quantum Theory*. Springer, 1983. DOI: 10.1007/3-540-12732-1. URL: https://doi.org/10.1007/3-540-12732-1.

[7] Géza Tóth and Iagoba Apellaniz. "Quantum metrology from a quantum information science perspective". In: *Journal of Physics A: Mathematical and Theoretical* 47.42 (2014), p. 424006. DOI: 10.1088/1751-8113/47/42/424006. URL: https://doi.org/10.1088/1751-8113/47/42/424006.

[8] Koenraad Audenaert. *Quantum Statistical Inference*. Imperial College London. Lecture Notes, available at https://www.imperial.ac.uk/media/imperial-college/research-centres-and-groups/theoretical-physics/msc/current/QuantumStatisticalInference.pdf. 2014.

[9] Luis A. Correa, Mohammad Mehboudi, Gerardo Adesso, and Anna Sanpera. "Low-temperature thermometry can be enhanced by strong coupling". In: *Physical Review Letters* 114.22 (2015), p. 220405. DOI: 10.1103/PhysRevLett.114.220405. URL: https://doi.org/10.1103/PhysRevLett.114.220405.

[10] T. M. Stace. "Quantum limits of thermometry". In: *Physical Review A* 82.1 (2010), p. 011611. DOI: 10.1103/PhysRevA.82.011611. URL: https://journals.aps.org/pra/abstract/10.1103/PhysRevA.82.011611.

[11] M. Jarzyna and M. Zwierz. "Quantum interferometry with and without an external phase reference". In: *Physical Review A* 92.3 (2015), p. 032112. DOI: 10.1103/PhysRevA.92.032112. URL: https://link.aps.org/doi/10.1103/PhysRevA.92.032112.

[12] Eduardo Martín-Martínez, Andrzej Dragan, Robert B. Mann, and Ivette Fuentes. "Berry phase quantum thermometer". In: *New Journal of Physics* 15 (2013), p. 053036. DOI: 10.1088/1367-2630/15/5/053036. URL: https://doi.org/10.1088/1367-2630/15/5/053036.

[13] Carlos Sabín, Andrew White, Lucia Hackermüller, and Ivette Fuentes. "Impurities as a quantum thermometer for a Bose–Einstein condensate". In: *Scientific Reports* 4 (2014), p. 6436. DOI: 10.1038/srep06436. URL: https://doi.org/10.1038/srep06436.

[14] Heinz-Peter Breuer and Francesco Petruccione. *The Theory of Open Quantum Systems*. Oxford: Oxford University Press, 2002. ISBN: 9780199213900.

[15] See Supplemental Material at http://link.aps.org/supplemental/10.1103/PhysRevLett.114.220405 for further details.

[16] Ricard Puig, Pavel Sekatski, Paolo Andrea Erdman, Paolo Abiuso, John Calsamiglia, and Martí Perarnau-Llobet. "From dynamical to steady-state many-body metrology: Precision limits and their attainability with two-body interactions". In: *arXiv preprint* 2412.02754 (2024). https://arxiv.org/abs/2412.02754. arXiv: 2412.02754.

[17] N. Anto-Sztrikacs, H. J. D. Miller, A. Nazir, and D. Segal. "Bypassing thermalization timescales in temperature estimation using prethermal probes". In: *Physical Review A* 109 (2024), p. L060201. DOI: 10.1103/PhysRevA.109.L060201.

[18] Wai-Keong Mok, Kishor Bharti, Leong-Chuan Kwek, and Abolfazl Bayat. "Optimal probes for global quantum thermometry". In: *arXiv preprint* 2010.14200 (2020). https://arxiv.org/abs/2010.14200 arXiv: 2010.14200.